Published September 22, 2015

Original Research

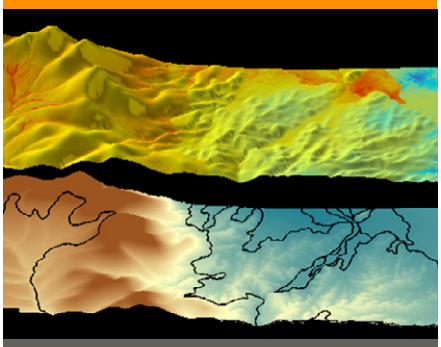

We applied spatial predictions of physical soil properties to a pedotransfer function to predict hydraulic properties at high resolution in a semiarid landscape. Estimated soil properties explained patterns of vegetation dynamics.

Application of Spatial Pedotransfer Functions to Understand Soil Modulation of Vegetation Response to Climate

Matthew R. Levi,* Marcel G. Schaap, and Craig Rasmussen

A fundamental knowledge gap in understanding land–atmosphere interactions is accurate, high-resolution spatial representation of soil physical and hydraulic properties. We present a novel approach to predict hydraulic soil parameters by combining digital soil mapping techniques with pedotransfer functions (PTFs) and demonstrate that simple derived quantities are related to observed spatial patterns in ecosystem production during the North American Monsoon. Landsat reflectance and elevation data were used to predict physical soil properties at a 5-m spatial resolution for a semiarid landscape of 6265 ha using regression kriging. Resulting soil property maps were applied to the Rosetta PTF to predict saturated hydraulic conductivity and water retention parameters from which approximate water residence times were derived. Estimated idealized residence time for water lost to the deeper vadose zone and evapotranspiration corresponded to vegetation response. Antecedent precipitation was more important for explaining the relationships between modeled soil properties and vegetation response than the amount of monsoon precipitation. Increased spring precipitation before the monsoon produced stronger negative correlations with hydraulic conductivity and stronger positive correlations with plant available water. Modeled water residence times explained the patterns of vegetation and landscape morphology validating our approach as a method of producing functional spatial PTFs. Linking digital soil mapping with Rosetta led to predictions of hydraulic soil properties that were more closely related to vegetation dynamics than the data available in the Soil Survey Geographic (SSURGO) soil database.

Abbreviations: MSAVI2, modified soil adjusted vegetation index, NMSE, normalized mean square error; PTF, pedotransfer function; SSURGO, Soil Survey Geographic Database; WRT, water retention time.

M.R. Levi, USDA-ARS Jornada Experimental Range, MSC 3JER, Box 30003, New Mexico State University, Las Cruces, NM 88003; M.G. Schaap and C. Rasmussen, University of Arizona, Department of Soil, Water, and Environmental Science, 1177 E. Fourth St., Shantz Bldg., Room 429, Tucson, AZ 85721-0038. *Corresponding author (mrlevi21@email.arizona.edu).

Vadose Zone J.
doi:10.2136/vzj2014.09.0126
Received 25 Sept. 2014.
Accepted 25 June 2015.

© Soil Science Society of America
5585 Guilford Rd., Madison, WI 53711 USA.
All rights reserved.

Representation of hydraulic soil properties across multiple scales is arguably the most important challenge for predicting soil moisture dynamics at landscape scales (Mohanty, 2013). When soil moisture is limiting, it exerts first-order control on land–atmosphere water and energy exchange (Seneviratne et al., 2010), particularly in semiarid ecosystems. Therefore, the interaction of precipitation events and hydraulic soil properties controls the partitioning between infiltration and runoff, the soil water dynamics in semiarid systems (Lauenroth and Bradford, 2012), and consequently, the productivity of shallow rooted vegetation (Shepard et al., 2015). In semiarid regions, surface soils experience the greatest flux in soil moisture following precipitation events, and it has been suggested that surface soils serve as the primary reservoir for water storage (Kurc and Small, 2004). Here, we examine how surface and subsurface soil property variability modulates the spatial and temporal distribution of aboveground vegetation productivity in a semiarid ecosystem in response to the North American Monsoon.

Traditional soil maps, in combination with topography, have provided the best available information for evaluating landscape-scale processes such as water cycling and vegetation change for nearly a century. Development of soil maps was often limited by time and

resource constraints, which translated to relatively coarse-scaled information for input to detailed hydrology models. To address the needs of detailed soil information, more focus has recently been directed to digital soil mapping as a tool to provide high-resolution soil data products that characterize spatial patterns with acceptable statistical confidence. Digital soil mapping utilizes a variety of spatial prediction techniques for estimating soil attributes (Grunwald, 2009) and has tremendous potential to address the need for site-specific soil properties in land surface modeling (Sanchez et al., 2009). This technique incorporates geographic information system modeling with conceptual models of soil formation like the one proposed by Jenny (1941) that identifies parent material, climate, biota, relief, and time as factors that control soil formation (McBratney et al., 2003). Surface reflectance obtained from remote sensing platforms (e.g., Landsat) and elevation-derived topographic indices are common inputs to digital soil mapping models (Hengl et al., 2007b; Moore et al., 1993; Nield et al., 2007) and allow quantitative estimation of soil and landscape properties through a variety of empirical and statistical techniques (Minasny et al., 2008; Saadat et al., 2008). Surface reflectance methods utilize soil reflectance relationships that are unique for different soil types, whereas topographic indices incorporate landscape features important for quantifying major energy inputs to the system (i.e., water and solar radiation).

One digital soil mapping approach that has received increased attention in recent years is regression kriging (Bishop and McBratney, 2001; Carre and Girard, 2002; Hengl et al., 2007a; Levi and Rasmussen, 2014; Li, 2010; Motaghian and Mohammadi, 2011). Regression kriging is a hybrid spatial interpolation technique that combines regression of environmental covariates and measured soil properties with ordinary kriging of the regression residuals (Hengl et al., 2004; Odeha et al., 1994). This approach can capture soil–landscape relationships not currently discernable from standard soil survey maps (Levi and Rasmussen, 2014). The incorporation of topographic variables is especially important for developing PTFs at landscape scales because hydraulic soil properties are strongly influenced by topography (Herbst et al., 2006; Leij et al., 2004; Rawls and Pachepsky, 2002; Sharma et al., 2006).

PTF models have been widely used to characterize soil hydraulic properties, by relating easy-to-obtain soil properties to hard-to-measure properties such as saturated hydraulic conductivity and infiltration rate, because direct measurement is expensive and time consuming (Hadzick et al., 2011; McBratney et al., 2006; Schaap and Leij, 1998; Schaap et al., 2001; Vereecken et al., 2010; Wosten et al., 1995, 2001). These models can be used to explore changes in the water balance as a function of management scenarios (Nemes et al., 2006); however, extrapolation of point measurements of in situ hydraulic parameters to unknown locations is limited because of their low spatial and temporal resolution (Tseng and Jury, 1993). Although relationships between hydraulic parameters and soil predictors are affected by spatial scale (Zeleke and Si, 2005), geostatistical models have been used to extrapolate measured hydraulic properties at points across the landscape to unknown locations (Liao et al., 2011; Motaghian and Mohammadi, 2011). Recent advances in PTF research have begun to incorporate remotely sensed auxiliary data directly into a PTF model to estimate soil water characteristics across spatial scales (Jana and Mohanty, 2011; Sharma et al., 2006; Smettem et al., 2004); however, the applications of digital soil mapping tools for vadose zone modeling are underutilized (Minasny et al., 2013) and the development of spatial PTFs has been minimal (McBratney et al., 2003). Few studies have linked digital soil mapping with PTFs to predict the spatial extent of hydraulic soil properties (Ugbaje and Reuter, 2013). Gutmann and Small (2010) proposed a need for landscape hydraulic properties instead of soil hydraulic properties to provide spatially accurate estimates of hydraulic parameters and present a method of incorporating remotely sensed data as a means to achieve this. Thus, a critical knowledge gap in the development of high-resolution models of surface processes is functional PTF models that can be applied across spatial scales.

We present a novel method for applying PTFs to high-resolution soil maps to improve predictions of vegetation response to soil and climate variation. Specific objectives included (i) predict key physical soil properties across the landscape using remotely sensed reflectance and elevation data and (ii) apply predicted soil properties to PTFs for estimation of water residence time at a landscape scale to better understand soil water dynamics. Our primary hypothesis was that digital soil mapping coupled with PTF derived proxies for soil water residence time will explain remotely sensed vegetation dynamics.

Materials and Methods

Study Area

The study area represents a sub-region of a recently mapped soil survey area (AZ673 Graham County, AZ, southwestern part) of approximately 160,000 ha located 30 km north of the town of Wilcox in southeastern Arizona (Fig. 1). The larger area includes a wide elevation gradient ranging from 910 to 1970 m asl with adjacent mountain ranges to the east and west that have maximum elevations of 3267 and 2336 m, respectively, that strongly influence soil–landscape relationships. Soil prediction focused on a smaller area of interest of approximately 6265 ha and an elevation gradient of 1273 to 1655 m asl (Fig. 1). This area was selected because it represents the variability of landscape positions, geology, surface reflectance, and soils found in the surrounding areas. Soils in the study area are mapped as Argiustolls in the western portion of the study area, Paleargids and Haplocambids in the eastern portion, Haplogypsids and Gypsitorrerts in the central portion, and Torrifluvents, Torriorthents, and riverwash in the drainages, with areas of rock outcrop distributed throughout portions of the upland landscape positions (Soil Survey Staff, 2011).

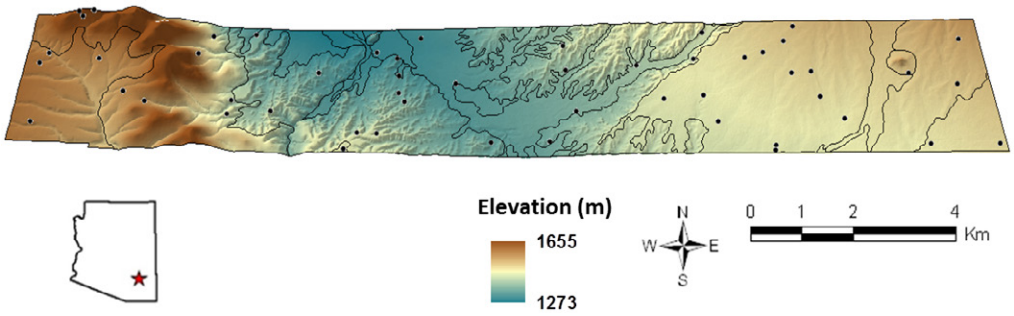

Fig. 1. Location of the study area in southeastern Arizona and elevation gradient for the area of interest. Black lines represent published soil survey delineations, and black points represent the location of 52 sampling sites used for soil prediction.

Sedimentary basin fill deposits, including dissected and inset alluvial fans and fan terraces, cover the study area and range in age from Holocene to early Miocene (~20 Ma) materials (Richard et al., 2000; Wilson and Moore, 1958). Areas to the east consist of large, gently sloping alluvial fans formed from Middle Proterozoic granitic rocks (1400–1450 Ma) and Early Proterozoic metamorphic rocks (1600–1800 Ma), that is, metasedimentary, metavolcanic, and gneissic rocks, while basin fill deposits in the western portion of the study area consist of material eroded from Middle Miocene to Oligocene age volcanic rocks (11–38 Ma), that is, andesite, rhyolite, and basalt, which are expressed on the landscape as a large alluvial fan composed of rhyolitic parent material and an area of hills formed of basalt. Pliocene to Middle Pleistocene age lacustrine deposits that contain abundant soluble salts including carbonates and gypsum occupy the center of the survey area (Fig. 1) (Melton, 1965). The major drainage network drains to the N–NW and stream channels are actively cutting back into the lacustrine sediments.

Variation in elevation, landform, and soils supports a diverse range of vegetation types across the study area. This area occupies the transition zone between the Sonoran and Chihuahuan Deserts, which differ in their annual precipitation regimes and dominant vegetation communities (Brown, 1994; Neilson, 1987). The study area is composed of semi-desert grassland (Brown and Lowe, 1994) and includes a variety of grasses, forbs, shrubs, leaf succulents, and cacti (Brown, 1994).

The climate of the study area is semiarid with mean annual precipitation that ranges from 403 to 472 mm and has a bi-modal distribution with maximum rainfall during the summer and winter months (PRISM Climate Group, Oregon State University, http://www.prism.oregonstate.edu, 2008). The North American Monsoon system controls the patterns of summer precipitation and varies at inter-annual and decadal scales (Sheppard et al., 2002). For comparisons of precipitation patterns in this study we have identified three seasons of the year to reflect the precipitation pulses important for vegetation response in the region: spring includes 1 January to 14 June, monsoon spans 15 June to 30 September, and fall includes 1 October to 31 December. The mean annual air temperature ranges from 16 to 17°C with the average minimum temperature ranging from 9 to 10°C and the average maximum temperature ranging from 23 to 25°C. The soil temperature regime is thermic (15–22°C). Soil moisture regimes include aridic and ustic, with the transition between the two occurring in the foothills of the neighboring mountain ranges (Soil Survey Staff, 2011).

We obtained daily precipitation data for the years 1987 to 2011 from the nearby Bonita meteorological station (~15 mi away), which is part of the Arizona Meteorological Network (http://ag.arizona.edu/azmet/index.html). Seasonal precipitation data were summarized between Landsat scenes to reflect actual vegetation responses between image dates and classified as spring, monsoon, and fall to approximate the standardized dates described above (the section "Relating Hydraulic Parameters to Vegetation Response" below provides more details of Landsat data).

Field Sampling and Laboratory Analysis

This project consisted of a data-driven approach to predicting physical and hydraulic soil properties. A sampling design derived from an iterative principal component data reduction and a conditioned Latin Hypercube routine was used to maximize model performance by identifying 52 sampling locations that represented variability in both feature space and geographic space (Minasny and McBratney, 2006). Details of the sampling design can be found in Levi and Rasmussen (2014). Figure 2 provides a conceptual workflow of the soil prediction model, the PTF model, and the linkage of these elements with vegetation indices derived from the Landsat remote sensing platform.

Soils were sampled by genetic soil horizons to a depth of 0 to 30 cm in April and May of 2011. Percentages of coarse fragments were determined on a volume basis by ocular methods, and soil samples were transported to the lab for further analysis. Air-dried soils <2 mm were prepared for particle size analysis with pretreatments of sodium acetate (NaOAc [pH 5]) to remove soluble salts and sodium hypochlorite (NaOCl [pH 9.5]) to remove organic matter (Jackson, 2005). After dispersion with sodium hexametaphosphate, soil particle size distribution was determined using a Beckman Coulter LS 13 320 Laser Diffraction Particle Size Analyzer.

Soil Prediction Models

Soil properties from surface and subsurface horizons were modeled separately using regression kriging. Variables were transformed

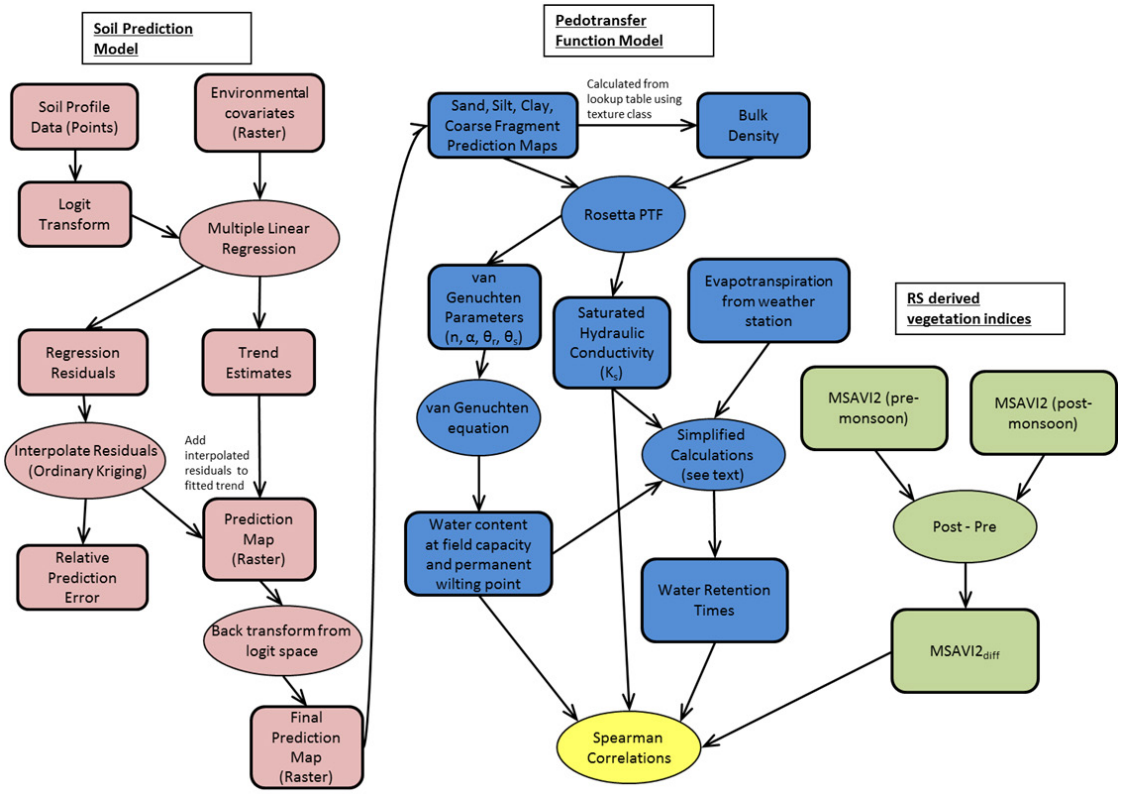

Fig. 2. Conceptual workflow for spatial pedotransfer function. Items in oval-shaped elements represent analysis procedures, and items in rounded squares are either final or intermediate data products. MSAVI2, modified soil adjusted vegetation index; $MSAVI2_{diff}$, the difference between MSAVI2 for post- and pre-monsoon for each year; PTF, pedotransfer function; RS, remote sensing.

with a logit transformation using the "boot" package in R (Canty and Ripley, 2011) to approximate a normal distribution for each dataset where

$$z_{++} = \ln\left(\frac{z^+}{1-z^+}\right);\ 0 < z^+ < 1 \qquad [1]$$

and z_{++} is the logit transformed variable, z^+ is the target variable standardized to the 0 to 1 range,

$$z_+ = \frac{z - z_{\min}}{z_{\max} - z_{\min}};\ z_{\min} < z < z_{\max} \qquad [2]$$

and $z_{\min}$ and $z_{\max}$ are the minimum and maximum values of z (Hengl et al., 2004). Percentages of sand, silt, clay, and coarse fragments were reported as a decimal.

Backward stepwise linear regression was performed using the "MASS" package in R (Venables and Ripley, 2002), and model selection was determined by minimizing the Akaike information criterion (Akaike, 1974). Independent variables used to predict soil properties included latitude, longitude, soil map units, and principal components of selected covariate data. Environmental covariate data used in soil prediction models were derived from one Landsat 7 scene collected on 12 Sept. 2000 and a digital elevation model derived from interferometric synthetic aperture radar with 5-m spatial resolution. The final set of covariate data included Landsat indices (Boettinger et al., 2008) of B3/B2, calcareous sediment index (B5 – B2)/(B5 + B2), and SAGA wetness index (Boehner et al., 2002). Ordinary kriging of the soil property residuals was performed with automatic variogram fitting using the automap package in R (Hiemstra et al., 2009). Regression equations were applied to the raster layers of predictor variables using the "raster" package in R (Hijmans and van Etten, 2011) and subsequently added to kriged residuals.

The model fit for each soil property was evaluated with a leave-one-out cross-validation of observed and predicted values of each variable. Untransformed values of observed and predicted variables were compared with Pearson correlation coefficients and the normalized mean square error (NMSE)

$$\mathrm{NMSE} = \frac{\frac{1}{n}\sum_{i=1}^{n}(p_i - o_i)^2}{s^2} \qquad [3]$$

where n is the number of observations, p_i is the predicted value at location i, o_i is the observed value at location i, and s^2 is the variance of the observed samples (Li and Heap, 2011). We followed

a regression kriging approach similar to Levi and Rasmussen (2014), but added latitude, longitude, and soil map units to the three principal components of environmental covariates. These predictors were not previously used in Levi and Rasmussen (2014) because the soil predictions were completed independently of soil survey map units and compared with soil survey. Here we developed a hybrid set of models that incorporated soil survey map units.

Pedotransfer Function and Derived Parameters

We used the Rosetta program (Schaap et al., 2001) to apply PTF models to the predicted soil physical properties described above. Rosetta is based on neural network analyses and combines a bootstrap technique to obtain the probability distribution of hydraulic parameters (Schaap and Leij, 1998). The van Genuchten (1980) water retention parameters and saturated hydraulic conductivity (K_s) were modeled separately for surface ($K_{s,sur}$) and subsurface soils ($K_{s,sub}$). Input to the model included percentages of sand, silt, clay, total coarse fragments (CF_total), and bulk density. Predicted values of sand, silt, and clay were normalized to total 100% and the soil texture class was assigned using the "soiltexture" package in R (Moeys and Shangguan, 2011). Bulk density was estimated for each resulting soil texture class according to a modified version of the NRCS technical handbook (Soil Survey Staff, 2011) customized to Arizona soils. Output from Rosetta were used to determine water retention at field capacity (330-cm pressure head) and the permanent wilting point (15×10^3 cm pressure head) according to van Genuchten (1980):

$$\theta(h) = \theta_r + \frac{(\theta_s - \theta_r)}{\left[1+(\alpha h)^n\right]^{1-1/n}}, \quad [4]$$

where $\theta(h)$ is the volumetric water content ($cm^3\ cm^{-3}$) at pressure head h (cm), θ_r and θ_s are residual and saturated water contents, respectively ($cm^3\ cm^{-3}$), α (>0, in cm^{-1}) is related to air entry pressure, and n (>1) is a measure of pore size distribution (van Genuchten, 1980; van Genuchten and Nielsen, 1985).

Unlike the soil prediction model, we were not able to validate PTF estimates of the van Genuchten (1980) parameters and K_s with field or laboratory observations because of experimental and financial constraints. Instead, we used model predictions of texture from the leave-one-out cross-validation ("Soil Prediction Models" section) as input for the PTF and compared the results with PTF estimates for the observed 52 field locations. Goodness-of-fit statistics included Pearson correlation and NMSE and provide an indication about the accuracy of the "texture model" in terms of hydraulic parameters.

Instead of applying a complex land surface model that would model vegetation productivity directly, we defined three simple metrics that can be used to relate soil property-related hydrologic quantities to landscape features and spatially variable vegetation response to meteorological forcing. These metrics included plant available water, water residence time as a function of gravitational water loss to the deeper vadose zone, and water residence time as a function of water loss to evapotranspiration. Each one of the metrics was defined in a very simple manner that is unlikely to represent the system exactly. However, the main purpose of this work was to find correlations between the soil-based metrics and remotely sensed vegetation productivity that can help inform future land surface modeling.

Plant available water was defined for the surface (PAW_{sur}) and subsurface (PAW_{sub}) layers as the difference between volumetric water content (θ) at field capacity (here defined as $h = -330$ cm) and the permanent wilting point (taken as $h = -15 \times 10^3$ cm). Effective plant available water for the observed profile (PAW_{eff}) was calculated as

$$PAW_{eff} = PAW_{sur} * T_{sur} + PAW_{sub} * T_{sub} \quad [5]$$

where T_{sur} and T_{sub} are the relative thickness of surface and subsurface soil layers ($T_{sur} + T_{sub} = 1$). Values for PAW_{eff} estimate the amount of water theoretically accessible to vegetation: water stored between saturation and field capacity will typically drain away rapidly, and water held beyond the wilting point is inaccessible because of strong capillary or absorptive forces. Effective plant available water provides a maximum storage capacity that is infrequently reached in the semiarid conditions of the study area.

The first residence time metric, WRT_{FC}, is the time required to drain a soil from saturation to field capacity and is useful for gauging how quickly a saturated soil drains vertically to the deeper vadose zone or laterally to streams. WRT_{FC} is calculated as

$$WRT_{FC} = \frac{\theta_{s,eff} - \theta(h=330)_{eff}}{K_{s,eff}} \quad [6]$$

where $K_{s,eff}$ is the effective K_s of the 30-cm profile, which is calculated as

$$\frac{1}{K_{s,eff}} = \frac{T_{sur}}{K_{s,sur}} + \frac{T_{sub}}{K_{s,sub}} \quad [7]$$

$K_{s,sur}$ and $K_{s,sub}$ are the saturated hydraulic conductivity of surface and subsurface soil layers. The above definition is somewhat unrealistic in that it assumes that hydraulic conductivity does not decrease between saturation and field capacity. In fact, it is likely that unsaturated hydraulic conductivity decreases stronger for coarse-textured soil and less for fine textured soil because of the shape factors α and n in the van Genuchten (1980) equation (Eq. [4]). As a result of the simplification, WRT_{FC} will provide underestimates of the real drainage time from saturation to

field capacity; conversely, usage of a mean unsaturated hydraulic conductivity at field capacity would lead to overestimates of the residence time. For the purposes of this study, however, the above definition of WRT_{FC} will suffice for producing values that are useful for non-parametric correlation with remotely sensed data.

The second residence time metric, WRT_{ET}, assumes that vertical or lateral drainage ceases at field capacity and that water can only be lost through evapotranspiration. WRT_{ET} is calculated according to

$$WRT_{ET} = \frac{PAW_{eff}}{0.63} \quad [8]$$

where PAW_{eff} is the effective plant available water and 0.63 is the average daily reference evapotranspiration rate (cm d^{-1}) for the monsoon period for the years 1998 to 2004 reported for the nearby Bonita meteorological station. The usage of the daily reference transpiration likely leads to underestimation of WRT_{ET} because vegetation coverage is not 100% (in fact it is spatially variable) and because the vegetation is unlikely to transpire at potential rates.

Relating Hydraulic Parameters to Vegetation Response

While remotely sensed proxies of vegetation greenness are not a direct measure of aboveground productivity, they are a useful metric for monitoring vegetation cover and response to climate. We used the modified soil adjusted vegetation index (MSAVI2) (Qi et al., 1994) to compare vegetation dynamics with spatial predictions of soil physical properties, hydraulic properties, and water retention time (WRT) metrics. This analysis was a direct test of how predicted hydraulic property estimates compared with vegetation patterns in this semiarid landscape.

Two Landsat images from each of 7 yr were selected to represent pre- and post-monsoon scenes (Table 1). All efforts were made to select scene dates from the same time each year; however, cloud cover of the study area prohibited the use of matching dates for each of the 7 yr. Landsat data were level 1G products with radiometric and geometric corrections. Each scene was atmospherically corrected for simple Rayleigh scattering using the Second Simulation of a Satellite Signal in the Solar System following Levi and Rasmussen (2011). Pixels representing earthen livestock tanks, cloud cover, and shadows were manually removed before the calculation of MSAVI2 using ArcGIS (Environmental Systems Research Institute, 2008). The equation for calculating MSAVI2 from Landsat is

$$MSAVI2 = \frac{2*B4+1-\sqrt{(2*B4+1)^2-8(B4-B3)}}{2} \quad [9]$$

where B4 and B3 correspond to the near infrared (band 4) and red (band 3) wavelengths, respectively.

Table 1. Details of Landsat scenes compared with predicted hydraulic soil properties.

Year	Pre-monsoon	Post-monsoon	Sensor†
1998	26 May	30 Aug.	LS 5 TM
1999	29 May	17 Aug.	LS 5 TM
2000	7 May	12 Sept.	LS 7 ETM+
2001	26 May	30 Aug.	LS 7 ETM+
2002	29 May	2 Sept.	LS 7 ETM+
2003	24 May	12 Aug.	LS 5 TM
2004	6 June	30 Aug.	LS 5 TM

† ETM, Enhanced Thematic Mapper Plus; LS, Landsat; TM, Thematic Mapper.

We used MSAVI2 as a proxy for estimating on-the-ground vegetation response to monsoonal precipitation for each of the 7 yr by taking the simple difference of the MSAVI2 from post- and pre-monsoon as

$$MSAVI2_{diff,i} = MSAVI2_{post,i} - MSAVI2_{pre,i} \quad [10]$$

where $MSAVI2_{diff,i}$ is the difference in MSAVI2 for year i, and $MSAVI2_{post,i}$ and $MSAVI2_{pre,i}$ are MSAVI2 for post- and pre-monsoon for year i, respectively. This approach is similar to the method used by Browning and Steele (2013) to evaluate vegetation dynamics in similar landscapes and vegetation types. We recognize that MSAVI2 is somewhat influenced by background soil conditions and does not therefore exclusively represent vegetation; however, we hereafter refer to the difference in MSAVI2 as the vegetation response.

Interpretations of the remotely sensed vegetation response are complicated by contributions of a variety of plant functional types (e.g., shrub, grass, forb) to the reflectance signal. For example, mesquite shrubs (*Prosopis* spp.) are deep-rooted plants common in many of the drainages across the study area that utilize available water from deep subsurface horizons that shallow-rooted grasses and succulents cannot reach (McAuliffe, 1995). Canopy greenness in shrub-dominated, semiarid ecosystems is strongly linked to deep soil moisture (Sanchez-Mejia et al., 2014). Therefore, it is expected that shrub green-up will be consistent in most years; hence, the main differences in MSAVI2 reflect grasses and forbs that rely on near-surface soil moisture for green-up. Spatial patterns of predicted soil properties were compared with the time series of MSAVI2 differences for each year by performing a Spearman rank correlation of all 5-m pixels of each predicted soil property to $MSAVI2_{diff}$ for each year.

We summarized seasonal rainfall between image dates of each year to reflect actual contributions of precipitation to each of the image dates. To enable accurate comparison of the precipitation patterns

Table 2. Summary statistics for measured clay, silt, sand, and total coarse fragments (CF_total) of surface and subsurface soils.

Surface (n = 52)						Subsurface (n = 51)				
Statistic	Clay	Silt	Sand	CF_total	Bulk density†	Clay	Silt	Sand	CF_total	Bulk density†
	%				g cm^{-3}	%				g cm^{-3}
Minimum	8.9	12.95	0.95	0	1.23	5.87	7.18	1.13	0	1.23
Maximum	70.13	46.8	75.43	55	1.43	81.65	50.75	86.95	85	1.53
Median	16.2	26.09	58.13	12.5	1.43	26.3	26.78	42.65	8.75	1.33
Range	61.23	33.85	74.48	55	0.2	75.78	43.57	85.83	85	0.3
SD	16.44	8.99	21.29	16.37	0.06	20.7	9.59	22.94	23.29	0.08
CV	0.71	0.33	0.43	0.89	0.05	0.59	0.36	0.6	1.24	0.06

† Bulk density statistics reflect modeled values.

to the vegetation trends depicted by Landsat images, we refer to these image-modified seasons.

Results and Discussion

Measured Soil Properties

Soils evaluated in this study area represent a wide range of particle sizes and coarse fragments (Levi and Rasmussen, 2014). Surface soil horizons had sand and clay percentages ranging from 1 to 75% and 9 to 70%, respectively (Table 2). Subsurface soils had even wider ranges of particle size with 1 to 87% sand and 6 to 82% clay (Table 2). The median clay percentage was higher in subsurface soils for 32 of the 52 sampled soils, which corresponded to the presence of argillic horizons with accumulation of clay-sized particles and that are indicative of stable landscapes. Median sand content was lower in the subsurface soils and silt content was similar for surface and subsurface soils. Percentages of coarse fragments (>2 mm) had a wider range of values in the subsurface (Table 2); however, the amount of coarse fragments was more evenly distributed in the surface soils (Table 2). Bulk density values ranging from 1.23 to 1.53 g cm^{-3} were assigned according to the soil texture class for all modeled locations and exhibited similar distributions for surface and subsurface soils (Table 2).

Predictive Soil Maps

Regression kriging produced estimates of soil properties that represented the variability of measured properties (Fig. 3) and corresponded to known soil–landscape patterns as represented in the published soil survey. The regression kriging models of Levi and Rasmussen (2014) showed significant agreement between predicted landscape variation and soil map unit boundaries, but did miss some key soil variation that was included in the polygonal soil maps, such as active riverwash and zones of floodplain with high silt content. Therefore, to improve the soil prediction models presented in Levi and Rasmussen (2014), here we included soil map units and spatial location via latitude and longitude as predictor variables. The incorporation of soil survey information in our

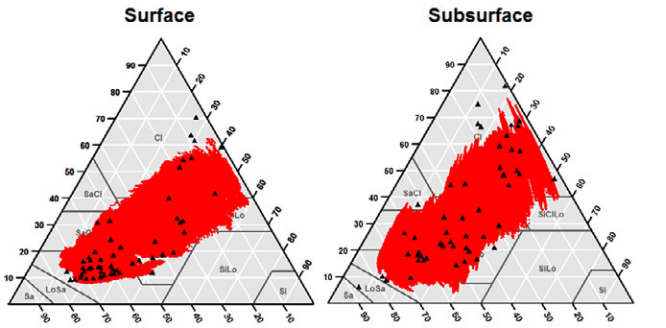

Fig. 3. Soil texture for surface and subsurface soil horizons modeled with regression kriging. Black triangles represent measured values. Each model was predicted for 2,505,109 pixels.

hybrid model significantly improved the prediction of subsurface soil properties when compared with a simpler model that only used principal components of environmental covariates. One of the main reasons the soil survey information improved predictions of subsurface soil properties is that soil survey relies heavily on subsurface diagnostic horizons, which can be difficult to discern with indices developed from surface soil reflectance. Pearson correlations from the leave-one-out cross-validation of soil texture ranged from 0.64 to 0.73 for surface soils and from 0.54 to 0.72 for subsurface soils (Table 3) (Levi and Rasmussen, 2014). Predictions of sand and clay percentage had the greatest Pearson correlation coefficient and lowest NMSE of all properties. Surface and subsurface property prediction models had similar goodness-of-fit statistics.

The wide range of soil texture in both surface and subsurface soil horizons reflected the variability of parent materials in the study area. Specifically, the western portion of the landscape is underlain by mafic, extrusive volcanic materials that favor formation of clay and red Fe-oxyhydroxide enriched soils, whereas the eastern portion of the study area is dominated by alluvial fans derived from felsic, granitic alluvium that favors formation of more coarse-grained soil textures. The regression component of the regression kriging method captured landscape features

Table 3. Goodness-of-fit statistics of observed and predicted values for all sampling locations for surface and subsurface soil properties predicted with regression kriging.†

	Surface (n = 52)		Subsurface (n = 51)	
Statistic	r	NMSE	r	NMSE
Clay‡	0.69	0.52	0.72	0.48
Sand‡	0.73	0.46	0.75	0.44
Silt‡	0.65	0.58	0.54	0.71
CF_total	0.64	0.64	0.68	0.57
A.thick	0.58	0.65	–	–
K_s	0.35	1.22	0.06	1.05
PAW	0.61	0.69	0.39	0.88
n	0.38	0.85	0.51	0.78
α	0.40	1.15	−0.06	1.26
θ_r	0.71	0.51	0.72	0.51
θ_s	0.63	0.60	0.77	0.43

† Pearson correlations (r) and normalized mean square error (NMSE) reflect results of leave-one-out cross-validation of untransformed values. A.thick is the thickness of the A horizon; CF_total is total coarse fragments; Clay, Sand, and Silt represent percent clay, sand, and silt; K_s is saturated hydraulic conductivity; n and α are fitting parameters of the van Genuchten equation; PAW is plant available water; and θ_r and θ_s are residual and saturated water contents, respectively. Hydraulic soil properties estimated with measured soil properties were compared with results of leave-one-out cross-validation.

‡ Sand, silt, and clay predictions were simultaneously scaled to sum to 100%.

important for delineating soil types as indicated by the correspondence between the predicted soil properties and the published soil survey. Predicted soil properties corresponded closely to topographic features, as a result of the regression kriging approach that included topographic information as a predictor. For example, percent slope was moderately correlated with surface clay (ρ = 0.50), surface coarse fragments (ρ = 0.75), subsurface clay (ρ = 0.49), and subsurface coarse fragments (ρ = 0.64).

Pedotransfer Function Estimates

Leave-one-out cross-validation of the hydraulic soil property estimates from Rosetta illustrated that models for surface soils were more accurate than subsurface soils. Pearson correlations ranged from 0.71 for θ_r to 0.35 for K_s in surface soils (Table 3). Subsurface models did not perform as well and had correlations ranging from −0.06 to 0.77. In particular, correlations for α and K_s were essentially zero, indicating that these pore-size related parameters cannot be estimated for the subsurface. The low correlations are likely due to three "outliers" that had observed sand percentages greater than 70%, but for which the predictive texture model predicted sand contents of around 50% (Fig. 4). As a consequence, PAW_{sub} estimates were also poor with a correlation coefficient of 0.39. A further investigation indicates that the three outliers are located in transition zones between landscape positions largely controlled by depositional or transport processes; all the other points are situated in more stable landscape positions. Barring the outliers in the cross-validation, there is a definite trend in predicted vs. observed $K_{s,sub}$ (Pearson correlation coefficient improved from 0.06 to 0.36 when three outliers were excluded), which suggests the potential for model improvement.

All predicted values of $K_{s,sur}$, $K_{s,sub}$, and $K_{s,eff}$ from Rosetta were within the range of values in databases summarized by Schaap and Leij (1998) and correspond well with measured values reported in other desert soils. Young et al. (2004) found that K_s was strongly dependent on the age of the geomorphic surface in sandy soils of the Mojave Desert with young soil surfaces having higher conductivity (200 cm d^{-1}) than older soils with more developed vesicular horizons (5 cm d^{-1}). Scanlon (1994) measured K_s values in soils with a wide range of textures from the Chihuahuan Desert of west Texas that were between 2 and 224 cm d^{-1}, and Adhikari et al. (2012) measured values of K_s between 25.7 and 1049 cm d^{-1} for very sandy soils in the Chihuahuan Desert near Las Cruces, NM.

The predicted hydraulic parameters also compared well with those reported in the SSURGO database, but more effectively maintained landscape features and spatial variability in soil properties modeled via regression kriging. Estimates of $K_{s,eff}$ values for the 0- to 30-cm soil profile ranged from 14 to 80 cm d^{-1} (Fig. 5), whereas SSURGO data ranged from 2 to 384 cm d^{-1} (Fig. 3). The range of reported of K_s values from SSURGO was much wider than our modeled estimates because our model did not adequately represent one of the soil map units composed of active riverwash and floodplain with gravelly coarse sand textures and very high K_s. The most notable spatial differences in between these data were the distinct boundaries at SSURGO soil map units relative to the more continuous predictions of K_s produced by the application of the Rosetta model to predicted soil properties. Predicted values for K_s were generally lower in the western third of the study area relative to higher values predicted in dissected alluvial fans in the central and eastern portion of the area. The SSURGO data indicated a similar pattern, albeit with much lower K_s in the western portion of the study area and limited areas of very high K_s values in drainages.

The trend in K_s from west to east may be explained by variation in soil parent material and resulting soil properties noted previously, whereby the western portion of the study area contains clay-rich soils derived from mafic volcanic materials and the eastern portion of the study area contains dissected alluvial fans derived from granitic materials that produce relatively sandy soils. The primary drainage network in the center of the study area was composed of a mixture of sandy and clayey soils, which contributed to more complex patterns of K_s. These contrasting parent materials across the study area were also reflected in other physical soil property differences.

Predicted PAW_{eff} in the 0- to 30-cm depth ranged from 2.4 to 5.8 cm of water. The spatial distribution of high and low values of PAW_{eff} was generally the opposite of K_s with more distinct

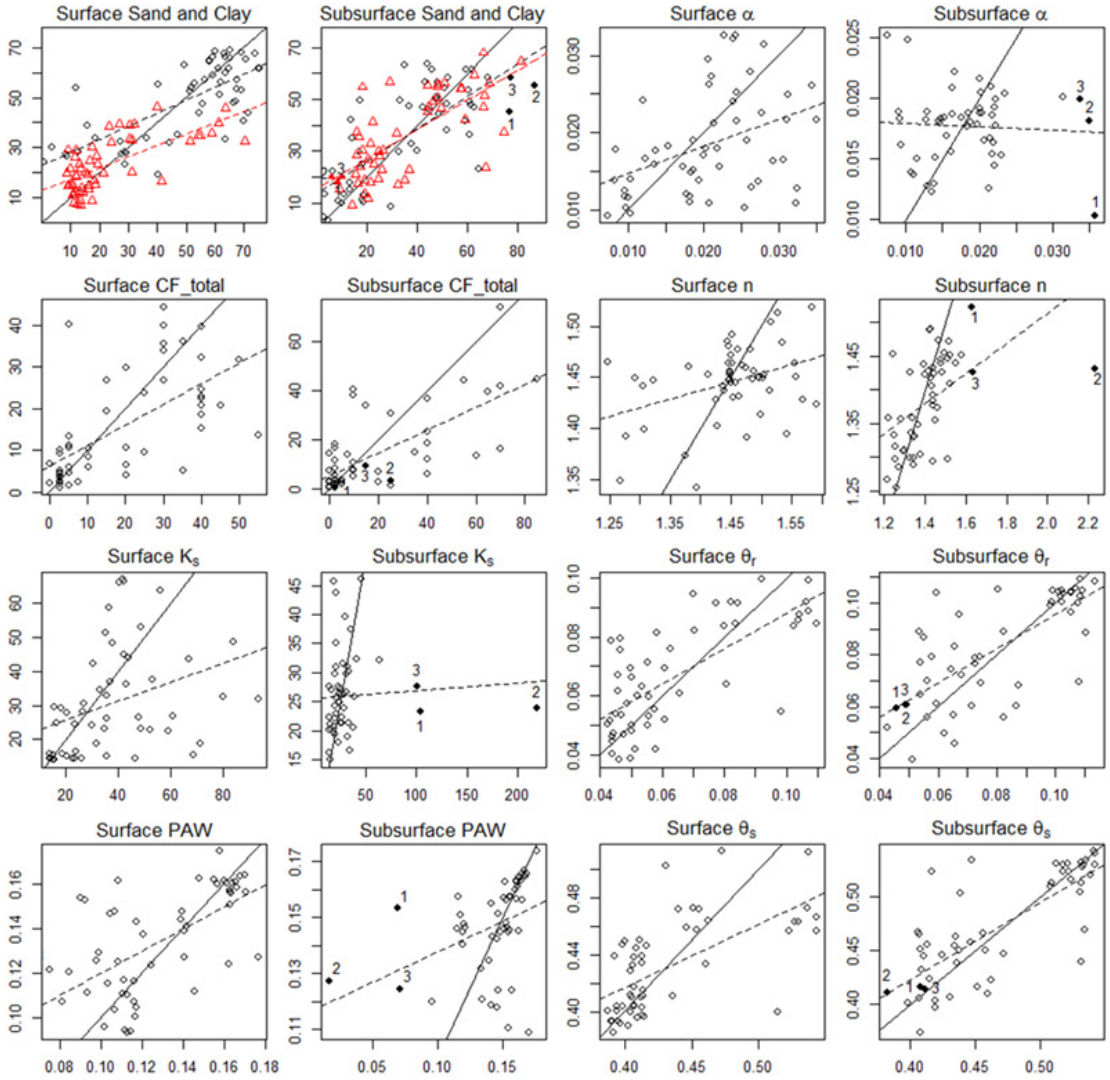

Fig. 4. Scatter plots showing goodness of fit between observed (*x* axis) and predicted (*y* axis) values for all sampling locations for surface and subsurface soil properties predicted with regression kriging. Predicted values are results of leave-one-out cross-validation. Sand and Clay represent percent sand and percent clay, CF_total is total coarse fragments, K_s is saturated hydraulic conductivity, PAW is plant available water, *n* and α are fitting parameters of the van Genuchten equation, and θ_r and θ_s are residual and saturated water contents, respectively. Hydraulic soil properties estimated with measured soil properties were compared with results of leave-one-out cross-validation. Solid line represents a 1:1 line, and dashed lines are fit lines. For plots of sand and clay, black circles represent sand and red triangles represent clay. Filled circles represent suspected outliers and were numbered to identify the same points in multiple plots.

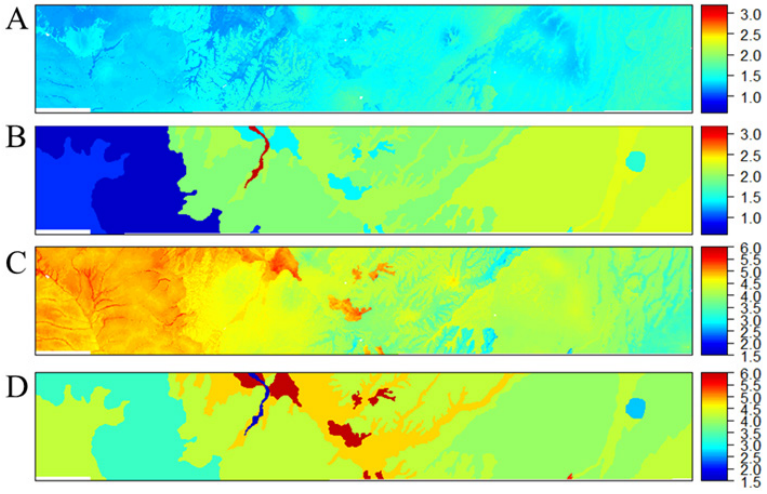

Fig. 5. Modeled effective saturated hydraulic conductivity ($\log_{10}$ [cm d^{-1}]) (A), effective saturated hydraulic conductivity ($\log_{10}$ [cm d^{-1}]) derived from the Soil Survey Geographic (SSURGO) database (B), modeled plant available water (cm cm^{-1}) (C), and plant available water (cm cm^{-1}) derived from SSURGO database (D). All values reflect a soil depth of 0 to 30 cm.

contrast between parent materials. The range of SSURGO derived PAW_{eff} values was very similar to Rosetta with estimates ranging from 1.5 to 6 cm of water (Fig. 5), further indicating that regression kriging of soil particle size coupled with the Rosetta PTF yielded results similar to published soil survey information.

Water Residence Time

The drainage based metric of water residence time, WRT_{FC}, was estimated as a fraction of a day with a maximum residence time of approximately 9 h. Estimates of WRT_{ET} for water lost to evapotranspiration at a rate of 6.3 mm d^{-1} were considerably longer ranging from 4 to 9 d (Fig. 6). Spatial patterns of both water residence time metrics were similar to patterns of PAW with longer residence times in the western portion of the study area and shorter residence times in the central and eastern portions and were directly related to the spatial arrangement of soil particle size classes across the landscape.

Topographic attributes were moderately correlated with modeled soil properties used to derive metrics of water retention and thus indirectly influenced estimates of WRT. Percent slope was positively correlated with WRT_{FC} ($\rho = 0.15$) and WRT_{ET} ($\rho = 0.42$). In contrast, wetness index was negatively correlated to both WRT_{FC} ($\rho = -0.08$) and WRT_{ET} ($\rho = -0.39$). These landscape patterns are in part due to parent material differences that control the physical and chemical soil properties. Higher relief in the western portion of the study area was associated with higher clay and longer residence times, whereas the granitic alluvial fans were much more flat. This explains the positive relationship between WRT and slope. Correlations between wetness index and percent slope were strongly negative, which resulted in the opposite trend found when comparing these topographic attributes to WRT. The influence of topography on hydraulic soil property variability found in this semiarid landscape supports previous studies that have identified similar relationships (Jana and Mohanty, 2012; Leij et al., 2004; Sharma et al., 2006).

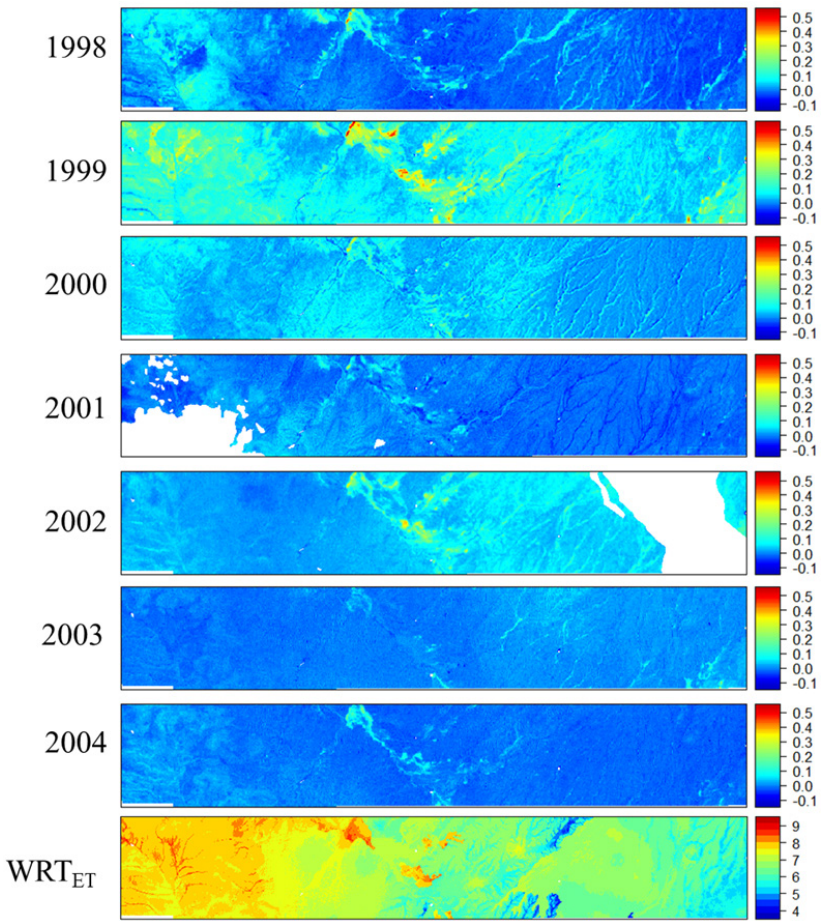

Fig. 6. Difference in MSAVI2 between pre- and post-monsoon Landsat scenes for 1998 to 2004. The greater difference in MSAVI2 represents more vegetation response from monsoonal precipitation. White areas in 2001 and 2002 represent no data due to clouds in Landsat scenes. WRT_{ET}, the time required (d) for all plant available water to be lost through evapotranspiration.

Vegetation Response to Soil Properties and Climate

Spatial patterns of vegetation response to the seasonal influx of precipitation resulting from the North American Monsoon were visible in $MSAVI2_{diff}$ images (Fig. 6 and 7). The greatest vegetation response was in 1999, 2000, and 2002 when monsoon rainfall was near the 25-yr mean and was preceded by very dry fall and spring conditions (Fig. 6 and 7). In contrast, 2001 and 2004 exhibited minimal vegetation response. These monsoon periods received only 53 and 62% of average monsoon precipitation after

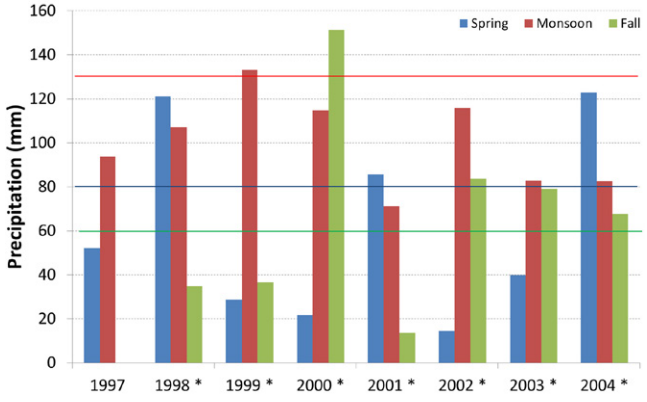

Fig. 7. Seasonal precipitation from a nearby meteorological station for 1997 to 2004 and 25 yr means for each season (horizontal lines). Spring includes 1 January to 14 June, monsoon is 15 June to 30 September, and fall includes 1 October to 31 December. Bars represent measured precipitation amounts between image dates in Table 1. Asterisks indicate years where Landsat-derived vegetation response during the monsoon period was compared with modeled soil hydraulic properties.

experiencing fall and spring precipitation in the previous seasons that well exceeded the means for those seasons. Essentially, wet seasons preceding the pre-monsoon image generally reduced the response of vegetation to monsoon rainfall, especially in years with dry monsoon conditions.

Soil particle size classes (sand, silt, clay) estimated with the regression kriging model exhibited correlation patterns with $MSAVI2_{diff}$ similar to those found for sand, silt, and clay from the SSURGO dataset (Table 4). Hydraulic soil properties (K_s and PAW) from modeled and SSURGO data showed similar relationships to vegetation response in some years; however, temporal patterns of correlation strength showed more variability than for soil particle size classes. Particle size classes in SSURGO were more strongly correlated with vegetation response than modeled values (e.g., surface sand and clay and subsurface sand). In contrast, modeled hydraulic properties showed stronger relationships with vegetation response than the same properties extracted from SSURGO. These results suggest that hydraulic soil property estimates in SSURGO can be improved by applying detailed predictions of particle size classes to PTFs. Although soil particle size classes and hydraulic properties showed similar correlation patterns, using PTFs converts physical soil variables like sand, silt, and clay into meaningful hydrological units and semi-quantitative soil moisture fluxes.

Vegetation response was positively correlated with soil properties related to water holding capacity. Correlations of $MSAVI2_{diff}$ with PAW from Rosetta were stronger than K_s in all years for both surface and subsurface depths, except in 1999 when $K_{s,sur}$ and PAW_{sur} showed nearly the same correlation strength. Both K_s and percent sand generally showed a negative relationship with vegetation response, whereas percent clay, percent silt, and PAW had a positive relationship with vegetation response. These trends held true for all years except 2002 and 2003. Interestingly, the sign of most of the correlations between $MSAVI2_{diff}$ and soil parameters flipped in 2002 and 2003 for the majority of properties in both modeled estimates and SSURGO; however, the mechanism responsible for this pattern is unclear.

One possible explanation for the unusual vegetation dynamics in 2002 and 2003 is explained by the lasting effects of drought conditions in 2001 (Fig. 7). The combined precipitation during the fall of 2001 and spring of 2002 was only 20% of the average for both seasons, lower than any other year. This seasonal drought likely constrained the vegetative production in response to the strong monsoon in 2002, possibly resulting from reduced tiller density of grass plants (Reichmann et al., 2013). In 2003, the sign of correlation patterns were very similar to those in 2002; however, the correlations were weaker. It is likely this pattern reflects the legacy effects of drought conditions in the fall of 2001 and spring of 2002 because vegetation responds to antecedent precipitation patterns with different lag times and previous year precipitation controls a significant fraction of the current-year production (Reichmann et al., 2013, Sala et al., 2012).

Table 4. Spearman correlation between the difference of modified soil adjusted vegetation index (MSAVI2) values (post-monsoon – pre-monsoon) and modeled soil properties ($MSAVI2_{diff\_Rosetta}$) and soil properties derived from the Soil Survey Geographic (SSURGO) database ($MSAVI2_{diff\_SSURGO}$) and hydraulic parameters for 7 yr.

	$MSAVI2_{diff\_Rosetta}$							$MSAVI2_{diff\_SSURGO}$							
Property†	1998	1999	2000	2001	2002	2003	2004	1998	1999	2000	2001	2002	2003	2004	Difference
A.thick	0.44	0.33	0.59	0.39	−0.51	−0.51	0.49								
$Sand_{sur}$	−0.51	−0.39	−0.46	−0.29	0.50	0.52	−0.47	−0.48	−0.50	−0.50	−0.38	0.28	0.49	−0.55	−0.01
$Silt_{sur}$	0.46	0.38	0.13	0.03	−0.28	−0.31	0.33	0.38	0.39	0.17	0.12	0.01	−0.23	0.35	0.04
$Clay_{sur}$	0.49	0.34	0.54	0.36	−0.59	−0.54	0.48	0.42	0.44	0.45	0.32	−0.39	−0.45	0.53	0.05
$Sand_{sub}$	−0.53	−0.28	−0.26	−0.33	0.59	0.42	−0.47	−0.44	−0.42	−0.51	−0.39	0.38	0.48	−0.54	−0.04
$Silt_{sub}$	0.48	0.43	0.23	0.18	−0.37	−0.38	0.42	0.10	0.19	0.48	0.30	0.06	−0.28	0.18	0.13
$Clay_{sub}$	0.45	0.21	0.21	0.31	−0.56	−0.36	0.43	0.35	0.27	0.35	0.27	−0.46	−0.40	0.44	0.00
$K_{s,sur}$	−0.50	−0.42	−0.47	−0.32	0.43	0.50	−0.49	−0.52	−0.50	−0.23	−0.24	−0.01	0.35	−0.54	0.10
PAW_{sur}	0.51	0.41	0.50	0.34	−0.48	−0.54	0.49	0.39	0.44	0.09	0.03	−0.01	−0.18	0.33	0.26
$K_{s,sub}$	−0.32	−0.06	−0.09	−0.13	0.29	0.22	−0.18	−0.27	−0.15	0.06	−0.01	0.00	0.15	−0.25	0.06
PAW_{sub}	0.49	0.25	0.24	0.32	−0.61	−0.44	0.45	−0.17	−0.02	0.22	0.01	−0.01	0.03	−0.09	0.32
WRT_{FC}	0.44	0.23	0.22	0.21	−0.39	−0.36	0.35								
WRT_{ET}	0.51	0.27	0.33	0.36	−0.62	−0.51	0.48								

† A.thick, A horizon thickness; Clay, percent clay; K_s, saturated hydraulic conductivity; PAW, plant available water; Sand, percent sand; Silt, percent silt; WRT_{ET}, water retention time for loss of plant available water to evapotranspiration at a rate of 0.63 cm d^{-1} for the 0- to 30-cm soil profile; WRT_{FC}, water retention time for gravitational loss of water at saturation to field capacity for the 0- to 30-cm soil profile. Subscripts $_{sur}$ and $_{sub}$ correspond to surface soil horizons and subsurface soil horizons. Difference is the difference of the sum of absolute value of correlation coefficients for all 7 yr in MSAVI2 and SSURGO.

Comparison of the antecedent rainfall to the correlation coefficients between hydraulic soil properties and vegetation response indicated that monsoon precipitation exhibited no significant relationship with correlation strength; however, antecedent rainfall was related to correlation strength and sign. Increased spring precipitation before $MSAVI2_{diff}$ analyses corresponded to negative relationships with $K_{s,sur}$ ($R^2 = 0.27$) and $K_{s,sub}$ ($R^2 = 0.56$) and positive relationships with PAW_{sur} ($R^2 = 0.27$) and PAW_{sub} ($R^2 = 0.47$). The same trends were found for the previous year's rainfall plus spring and monsoon rainfall in the measurement year to the correlation strength ($R^2 = 0.41$ for both $K_{s,sur}$ and PAW_{sur}). Comparing the cumulative antecedent rainfall from 2 yr also showed similar trends, but there was no relationship between rainfall amount and correlation beyond 2.5 yr. We found similar patterns for both surface and subsurface soils, which highlights the importance of antecedent rainfall and potential stored soil water for vegetative growth.

The relationships between surface and subsurface soil horizons and vegetation response varied across all properties in both modeled values and SSURGO data (Table 4). Properties derived from regression kriging and Rosetta indicated stronger relationships in surface horizons than for the corresponding subsurface horizon. Previous research has suggested surface soils (0–10 cm) in the southwestern United States are the dominant water reservoir in both grassland and shrubland sites (Kurc and Small, 2004, 2007). We found that PAW_{sur} showed stronger positive correlations to vegetation response than PAW_{sub} in 6 of the 7 yr (Table 4), indicating the importance of surface soil properties to vegetation in this system. Increased rates of evapotranspiration during the summer months limit the amount of moisture reaching subsurface soils, which potentially mutes the influence of subsurface soil property differences on vegetation response (Shepard et al., 2015). Modeled estimates of PAW_{sur} and PAW_{sub} were positively correlated with the vegetation response in 5 of the 7 yr, whereas PAW_{sub} from SSURGO data showed positive correlations with vegetation response in 3 yr. $K_{s,sur}$ and $K_{s,sub}$ showed an opposite pattern in both modeled values and SSURGO of negative correlations with vegetation response in most years. Estimates of WRT_{FC} and WRT_{ET} were positively correlated with vegetation response in 5 of the 7 yr.

The comparison of vegetation response to soil properties does not take into account the spatial redistribution of water from runoff or lateral movement of water in the soil. For example, Fig. 6 shows several large patches of strong vegetation response in 1999 and 2002, which reflect areas of big sacaton (*Sporobolis wrightii* Munro ex Scribn.), a large perennial bunchgrass that can grow nearly 2 m in height and grows in monotypic strands in broad floodplains in areas of southeastern Arizona (Casady et al., 2013). These patches of big sacaton are present in low-lying areas that are subject to flooding and likely experienced run-on water during the above average monsoon period in 1999 and 2002 (Fig. 7). Although present in other years, areas of sacaton were not as pronounced because of below average monsoon precipitation. Furthermore, these areas of green-up correspond to soil survey polygons with higher clay and silt content, which illustrates the importance of multi-temporal images in digital soil mapping efforts to capture spatiotemporal vegetation dynamics related to soil property variability across the landscape.

Relationships explained by WRT scenarios and independent landscape-scale drainage patterns and vegetation response agreed with our primary hypothesis that water residence times derived from the spatial PTFs showed significant correlations with remotely sensed vegetation dynamics, suggesting this approach can explain spatial distributions of important hydraulic properties that can contribute to landscape-scale hydrology modeling. Our results suggest the estimation of WRT explained vegetation response across a wide range of inter-annual precipitation patterns, which has strong implications for improving predictions of landscape-scale vegetation dynamics and ecosystem response to changing climate patterns in the Southwest.

Conclusions

Knowledge of the spatial distribution of key soil properties can aid our estimation of harder to measure hydraulic soil properties for improved models of soil moisture and vegetation dynamics. We presented a novel approach to predicting hydraulic soil parameters that incorporated digital soil mapping techniques and PTF modeling, which is useful for filling this knowledge gap. Estimates of WRT for gravitational loss of water from saturation to field capacity and continued loss of plant available water to evapotranspiration were modeled separately and corresponded to landscape-scale processes of drainage patterns and vegetation response. These concepts should be further developed to simultaneously model the loss of water to drainage and evapotranspiration to provide better estimates of available soil water. Furthermore, this approach does not account for nonlinear changes in hydraulic conductivity at unsaturated conditions and could be improved with more complex models of water flow; thus, we suggest future work should attempt to address this to advance spatial estimations of hydraulic soil properties. We provide a proof of concept for an approach to produce functional PTF models that can be applied spatially at landscape and regional scales and is validated against spatial patterning in vegetation response and landscape morphology. This work lays important groundwork for advancing the development of spatial PTFs to improve our understanding of how surface soil properties influence vegetation responses in semiarid systems. It is also important for informing future numerical models to quantify these processes in more detail. Findings presented here suggest digital soil mapping and hydrologic modeling techniques can be successfully integrated to better understand changes in soil–water–vegetation dynamics at landscape scales resulting from temporal precipitation patterns and ultimately help to guide land management in the face of changing climate patterns.

Acknowledgments

This research was supported by the USDA-NRCS of Arizona cooperative agreement 68-9457-8-466, NSF EAR/IF 0929850, and the Arizona Agricultural Experiment Station ARZT-1367190-H21-155. We thank S. Loheide and two anonymous reviewers for providing comments that improved the quality of this work.

References

Adhikari, P., M.K. Shukla, and J.G. Mexal. 2012. Spatial variability of hydraulic conductivity and sodium content of desert soils: Implications for management of irrigation using treated wastewater. Trans. ASABE 55:1711–1721. doi:10.13031/2013.42362

Akaike, H. 1974. New look at statistical-model identification. IEEE Trans. Autom. Control 19:716–723. doi:10.1109/TAC.1974.1100705

Bishop, T.F.A., and A.B. McBratney. 2001. A comparison of prediction methods for the creation of field-extent soil property maps. Geoderma 103:149–160. doi:10.1016/S0016-7061(01)00074-X

Boehner, J., R. Koethe, O. Conrad, J. Gross, A. Ringeler, and T. Selige. 2002. Soil regionalisation by means of terrain analysis and process parameterisation. In: E. Micheli, F. Nachtergaele, and L. Montanarella, editors, Soil classification 2001. Res. Rep. No. 7, EUR 20398 EN. European Soil Bureau, Ispra, Italy. p. 213–222.

Boettinger, J.L., R.D. Ramsey, J.M. Bodily, N.J. Cole, S. Kienast-Brown, S.J. Nield, A.M. Saunders, and A.K. Stum. 2008. Landsat spectral data for digital soil mapping. In: A.E. Hartemink, A. McBratney, and M.L. Mendonça-Santos, editors, Digital soil mapping with limited data. Elsevier, Amsterdam. p. 193–202.

Brown, D.E. 1994. Biotic communities: Southwestern United States and northwestern Mexico. Univ. of Utah Press, Salt Lake City.

Brown, D.E., and C.H. Lowe. 1994. Biotic communities of the Southwest. Univ. of Utah Press, Salt Lake City.

Browning, D.M., and C.M. Steele. 2013. Vegetation index differencing for broad-scale assessment of productivity under prolonged drought and sequential high rainfall conditions. Remote Sens. 5:327–341. doi:10.3390/rs5010327

Canty, A., and B. Ripley. 2011. boot: Bootstrap R (S-Plus) Functions.

Carre, F., and M.C. Girard. 2002. Quantitative mapping of soil types based on regression kriging of taxonomic distances with landform and land cover attributes. Geoderma 110:241–263. doi:10.1016/S0016-7061(02)00233-1

Casady, G.M., W.J.D. van Leeuwen, and B.C. Reed. 2013. Estimating winter annual biomass in the Sonoran and Mojave Deserts with satellite- and ground-based observations. Remote Sens. 5:909–926. doi:10.3390/rs5020909

Environmental Systems Research Institute. 2008. ArcGIS version 9.3. ESRI, Redlands, CA.

Grunwald, S. 2009. Multi-criteria characterization of recent digital soil mapping and modeling approaches. Geoderma 152:195–207. doi:10.1016/j.geoderma.2009.06.003

Gutmann, E.D., and E.E. Small. 2010. A method for the determination of the hydraulic properties of soil from MODIS surface temperature for use in land-surface models. Water Resour. Res. 46:W06520. doi:10.1029/2009WR008203

Hadzick, Z.Z., A.K. Guber, Y.A. Pachepsky, and R.L. Hill. 2011. Pedotransfer functions in soil electrical resistivity estimation. Geoderma 164:195–202. doi:10.1016/j.geoderma.2011.06.004

Hengl, T., G.B.M. Heuvelink, and D.G. Rossiter. 2007a. About regression-kriging: From equations to case studies. Comput. Geosci. 33:1301–1315. doi:10.1016/j.cageo.2007.05.001

Hengl, T., G.B.M. Heuvelink, and A. Stein. 2004. A generic framework for spatial prediction of soil variables based on regression-kriging. Geoderma 120:75–93. doi:10.1016/j.geoderma.2003.08.018

Hengl, T., N. Toomanian, H.I. Reuter, and M.J. Malakouti. 2007b. Methods to interpolate soil categorical variables from profile observations: Lessons from Iran. Geoderma 140:417–427. doi:10.1016/j.geoderma.2007.04.022

Herbst, M., B. Diekkrüger, and H. Vereecken. 2006. Geostatistical co-regionalization of soil hydraulic properties in a micro-scale catchment using terrain attributes. Geoderma 132:206–221. doi:10.1016/j.geoderma.2005.05.008

Hiemstra, P.H., E.J. Pebesma, C.J.W. Twenhöfel, and G.B.M. Heuvelink. 2009. Real-time automatic interpolation of ambient gamma dose rates from the Dutch radioactivity monitoring network. Comput. Geosci. 35:1711–1721. doi:10.1016/j.cageo.2008.10.011

Hijmans, R.J., and J. van Etten. 2011. raster: Geographic analysis and modeling with raster data. R package version 1.9-33. http://CRAN.R-project.org/package=raster (accessed 6 Apr. 2015).

Jackson, M.L. 2005. Soil chemical analysis: Advanced course. 2nd ed. Univ. of Wisonsin-Madison Libraries Parallel Press, Madison, WI.

Jana, R.B., and B.P. Mohanty. 2011. Enhancing PTFs with remotely sensed data for multi-scale soil water retention estimation. J. Hydrol. 399:201–211. doi:10.1016/j.jhydrol.2010.12.043

Jana, R.B., and B.P. Mohanty. 2012. On topographic controls of soil hydraulic parameter scaling at hillslope scales. Water Resour. Res. 48:W02518. doi:10.1029/2011WR011204

Jenny, H. 1941. Factors of soil formation: A system of quantitative pedology. 1st ed. McGraw-Hill, New York.

Kurc, S.A., and E.E. Small. 2004. Dynamics of evapotranspiration in semiarid grassland and shrubland ecosystems during the summer monsoon season, central New Mexico. Water Resour. Res. 40:W09305. doi:10.1029/2004WR003068

Kurc, S.A., and E.E. Small. 2007. Soil moisture variations and ecosystem-scale fluxes of water and carbon in semiarid grassland and shrubland. Water Resour. Res. 43:W06416. doi:10.1029/2006WR005011

Lauenroth, W.K., and J.B. Bradford. 2012. Ecohydrology of dry regions of the United States: Water balance consequences of small precipitation events. Ecohydrology 5:46–53. doi:10.1002/eco.195

Leij, F.J., N. Romano, M. Palladino, M.G. Schaap, and A. Coppola. 2004. Topographical attributes to predict soil hydraulic properties along a hillslope transect. Water Resour. Res. 40:W02407. doi:10.1029/2002WR001641

Levi, M.R., and C. Rasmussen. 2011. Considerations for atmospheric correction of surface reflectance for soil survey applications. Soil Surv. Horiz. 52:48–55. doi:10.2136/sh2011.2.0048

Levi, M.R., and C. Rasmussen. 2014. Covariate selection with iterative principal component analysis for predicting physical soil properties. Geoderma 219–220:46–57. doi:10.1016/j.geoderma.2013.12.013

Li, J., and A.D. Heap. 2011. A review of comparative studies of spatial interpolation methods in environmental sciences: Performance and impact factors. Ecol. Inform. 6:228–241. doi:10.1016/j.ecoinf.2010.12.003

Li, Y. 2010. Can the spatial prediction of soil organic matter contents at various sampling scales be improved by using regression kriging with auxiliary information? Geoderma 159:63–75. doi:10.1016/j.geoderma.2010.06.017

Liao, K.H., S.H. Xu, J.C. Wu, S.H. Ji, and Q. Lin. 2011. Assessing soil water retention characteristics and their spatial variability using pedotransfer functions. Pedosphere 21:413–422. doi:10.1016/S1002-0160(11)60143-4

McAuliffe, J.R. 1995. Landscape evolution, soil formation, and Arizona's grasslands. In: M.P. McClaran and T.R. Van Devender, editors, The desert grassland. Univ. of Arizona Press, Tucson. p. 100–129.

McBratney, A.B., B. Minasny, and R.V. Rossel. 2006. Spectral soil analysis and inference systems: A powerful combination for solving the soil data crisis. Geoderma 136:272–278. doi:10.1016/j.geoderma.2006.03.051

McBratney, A.B., M.L.M. Santos, and B. Minasny. 2003. On digital soil mapping. Geoderma 117:3–52. doi:10.1016/S0016-7061(03)00223-4

Melton, M.A. 1965. The geomorphic and paleoclimatic significance of alluvial deposits in southern Arizona. J. Geol. 73:1–38. doi:10.1086/627044

Minasny, B., and A.B. McBratney. 2006. A conditioned Latin hypercube method for sampling in the presence of ancillary information. Comput. Geosci. 32:1378–1388. doi:10.1016/j.cageo.2005.12.009

Minasny, B., A.B. McBratney, and S. Salvador-Blanes. 2008. Quantitative models for pedogenesis—A review. Geoderma 144:140–157. doi:10.1016/j.geoderma.2007.12.013

Minasny, B., B.M. Whelan, J. Triantafilis, and A.B. McBratney. 2013. Pedometrics research in the vadose zone—Review and perspectives. Vadose Zone J. 12(4). doi:10.2136/vzj2012.0141

Moeys, J., and W. Shangguan. 2011. soiltexture: Functions for soil texture plot, classification and transformation. R package version 1.2.6. http://CRAN.R-project.org/package=soiltexture

Mohanty, B.P. 2013. Soil hydraulic property estimation using remote sensing: A review. Vadose Zone J. 12(4). doi:10.2136/vzj2013.06.0100

Moore, I.D., P.E. Gessler, G.A. Nielsen, and G.A. Peterson. 1993. Soil attribute prediction using terrain analysis. Soil Sci. Soc. Am. J. 57:443–452. doi:10.2136/sssaj1993.03615995005700020026x

Motaghian, H.R., and J. Mohammadi. 2011. Spatial estimation of saturated hydraulic conductivity from terrain attributes using regression, kriging, and artificial neural networks. Pedosphere 21:170–177. doi:10.1016/S1002-0160(11)60115-X

Neilson, R.P. 1987. Biotic regionalization and climatic controls in western North-America. Vegetatio 70:135–147.

Nemes, A., J.H.M. Wosten, J. Bouma, and G. Varallyay. 2006. Soil water balance scenario studies using predicted soil hydraulic parameters. Hydrol. Processes 20:1075–1094 10.1002/hyp.5934. doi:10.1002/hyp.5934

Nield, S.J., J.L. Boettinger, and R.D. Ramsey. 2007. Digitally mapping gypsic and natric soil areas using Landsat ETM data. Soil Sci. Soc. Am. J. 71:245–252. doi:10.2136/sssaj2006-0049

Odeha, I.O.A., A.B. McBratney, and D.J. Chittleborough. 1994. Spatial prediction of soil properties from landform attributes derived from a digital elevation model. Geoderma 63:197–214. doi:10.1016/0016-7061(94)90063-9

Qi, J., A. Chehbouni, A.R. Huete, Y.H. Kerr, and S. Sorooshian. 1994. A modified soil adjusted vegetation index. Remote Sens. Environ. 48:119–126. doi:10.1016/0034-4257(94)90134-1

Rawls, W.J., and Y.A. Pachepsky. 2002. Using field topographic descriptors to estimate soil water retention. Soil Sci. 167:423–435. doi:10.1097/00010694-200207000-00001

Reichmann, L.G., O.E. Sala, and D.P.C. Peters. 2013. Precipitation legacies in desert grassland primary production occur through previous-year tiller density. Ecology 94:435–443. doi:10.1890/12-1237.1

Richard, S.M., S.J. Reynolds, J.E. Spencer, and P.A. Pearthree. 2000. Geologic map of Arizona. Map 35. Arizona Geological Survey, Phoenix. Scale 1:1,000,000.

Saadat, H., R. Bonnell, F. Sharifi, G. Mehuys, M. Namdar, and S. Ale-Ebrahim. 2008. Landform classification from a digital elevation model and satellite imagery. Geomorphology 100:453–464. doi:10.1016/j.geomorph.2008.01.011

Sala, O.E., L.A. Gherardi, L. Reichmann, E. Jobbagy, and D. Peters. 2012. Legacies of precipitation fluctuations on primary production: Theory and data synthesis. Philos. Trans. R. Soc. B. 367:3135–3144 doi:10.1098/rstb.2011.0347

Sanchez, P.A., S. Ahamed, F. Carre, A.E. Hartemink, J. Hempel, J. Huising, P. Lagacherie, A.B. McBratney, N.J. McKenzie, M.L. Mendonça-Santos, B. Minasny, L. Montanarella, P. Okoth, C.A. Palm, J.D. Sachs, K.D. Shepherd, T.-G. Vågen, B. Vanlauwe, M.G. Walsh, L.A. Winowiecki, and G.-L. Zhang. 2009. Digital soil map of the world. Science 325:680–681. doi:10.1126/science.1175084

Sanchez-Mejia, Z.M., S.A. Papuga, J.B. Swetish, W.J.D. van Leeuwen, D. Szutu, and K. Hartfield. 2014. Quantifying the influence of deep soil moisture on ecosystem albedo: The role of vegetation. Water Resour. Res. 50:4038–4053. doi:10.1002/2013WR014150

Scanlon, B.R. 1994. Water and heat fluxes in desert soils. 1. Field studies. Water Resour. Res. 30:709–719. doi:10.1029/93WR03251

Schaap, M.G., and F.J. Leij. 1998. Database-related accuracy and uncertainty of pedotransfer functions. Soil Sci. 163:765–779. doi:10.1097/00010694-199810000-00001

Schaap, M.G., F.J. Leij, and M.Th. van Genuchten. 2001. ROSETTA: A computer program for estimating soil hydraulic parameters with hierarchical pedotransfer functions. J. Hydrol. 251:163–176. doi:10.1016/S0022-1694(01)00466-8

Seneviratne, S.I., T. Corti, E.L. Davin, M. Hirschi, E.B. Jaeger, I. Lehner, B. Orlowsky, and A.J. Teuling. 2010. Investigating soil moisture–climate interactions in a changing climate: A review. Earth Sci. Rev. 99:125–161. doi:10.1016/j.earscirev.2010.02.004

Sharma, S.K., B.P. Mohanty, and J.T. Zhu. 2006. Including topography and vegetation attributes for developing pedotransfer functions. Soil Sci. Soc. Am. J. 70:1430–1440. doi:10.2136/sssaj2005.0087

Shepard, C., M.G. Schaap, M.A. Crimmins, W.J.D. van Leeuwen, and C. Rasmussen. 2015. Subsurface soil textural control of aboveground productivity in the US Desert Southwest. Geoderma Reg. 4:44–54. doi:10.1016/j.geodrs.2014.12.003

Sheppard, P.R., A.C. Comrie, G.D. Packin, K. Angersbach, and M.K. Hughes. 2002. The climate of the US Southwest. Clim. Res. 21:219–238. doi:10.3354/cr021219

Smettem, K., G. Pracilio, Y. Oliver, and R. Harper. 2004. Data availability and scale in hydrologic applications. In: Y. Pachepsky and W.J. Rawls, editors, Development of pedotransfer functions in soil hydrology. Elsevier, Amsterdam. p. 253–272.

Soil Survey Staff. 2011. Soil Survey Geographic (SSURGO) database for Graham County, Arizona, southwestern part. USDA-NRCS, Washington, DC. http://soildatamart.nrcs.usda.gov (accessed 30 Aug. 2011).

Tseng, P.H., and W.A. Jury. 1993. Simulation of field measruement of hydraulic conductivity in unsaturated hetrogeneous soil. Water Resour. Res. 29:2087–2099. doi:10.1029/93WR00578

Ugbaje, S.U., and H.I. Reuter. 2013. Functional digital soil mapping for the prediction of available water capacity in Nigeria using legacy data. Vadose Zone J. 12(4). doi:10.2136/vzj2013.07.0140

van Genuchten, M.Th. 1980. A closed-form equation for predicting the hydraulic conductivity of unsaturated soils. Soil Sci. Soc. Am. J. 44:892–898. doi:10.2136/sssaj1980.03615995004400050002x

van Genuchten, M.Th., and D.R. Nielsen. 1985. On describing and predicting the hydraulic properties of unsaturated soils. Ann. Geophys. 3:615–627.

Venables, W.N., and B.D. Ripley. 2002. Modern applied statistics with S. 4th ed. Springer, New York.

Vereecken, H., M. Weynants, M. Javaux, Y. Pachepsky, M.G. Schaap, and M.Th. van Genuchten. 2010. Using pedotransfer functions to estimate the van Genuchten–Mualem soil hydraulic properties: A review. Vadose Zone J. 9:795–820. doi:10.2136/vzj2010.0045

Wilson, E.D., and T. Moore. 1958. Geologic map of Graham and Greenlee Counties, Arizona. Arizona Bureau of Mines and the University of Arizona, Tucson. Scale 1:375,000.

Wosten, J.H.M., P.A. Finke, and M.J.W. Jansen. 1995. Comparison of class and continuous pedotransfer functions to generate soil hydraulic characteristics. Geoderma 66:227–237. doi:10.1016/0016-7061(94)00079-P

Wosten, J.H.M., Y.A. Pachepsky, and W.J. Rawls. 2001. Pedotransfer functions: Bridging the gap between available basic soil data and missing soil hydraulic characteristics. J. Hydrol. 251:123–150. doi:10.1016/S0022-1694(01)00464-4

Young, M.H., E.V. McDonald, T.G. Caldwell, S.G. Benner, and D.G. Meadows. 2004. Hydraulic properties of a desert soil chronosequence in the Mojave Desert, USA. Vadose Zone J. 3:956–963. doi:10.2136/vzj2004.0956

Zeleke, T.B., and B.C. Si. 2005. Scaling relationships between saturated hydraulic conductivity and soil physical properties. Soil Sci. Soc. Am. J. 69:1691–1702. doi:10.2136/sssaj2005.0072